Cell Death and Differentiation (2017) 24, 798–808
 1350-9047/17

www.nature.com/cdd

Intrinsic repair protects cells from pore-forming toxins by microvesicle shedding

Matthew Romero[1], Michelle Keyel[1], Guilan Shi[1,4], Pushpak Bhattacharjee[1,5], Robyn Roth[2], John E Heuser[3] and Peter A Keyel*[,1]

Pore-forming toxins (PFTs) are used by both the immune system and by pathogens to disrupt cell membranes. Cells attempt to repair this disruption in various ways, but the exact mechanism(s) that cells use are not fully understood, nor agreed upon. Current models for membrane repair include (1) patch formation (e.g., fusion of internal vesicles with plasma membrane defects), (2) endocytosis of the pores, and (3) shedding of the pores by blebbing from the cell membrane. In this study, we sought to determine the specific mechanism(s) that cells use to resist three different cholesterol-dependent PFTs: Streptolysin O, Perfringolysin O, and Intermedilysin. We found that all three toxins were shed from cells by blebbing from the cell membrane on extracellular microvesicles (MVs). Unique among the cells studied, we found that macrophages were 10 times more resistant to the toxins, yet they shed significantly smaller vesicles than the other cells. To examine the mechanism of shedding, we tested whether toxins with engineered defects in pore formation or oligomerization were shed. We found that oligomerization was necessary and sufficient for membrane shedding, suggesting that calcium influx and patch formation were not required for shedding. However, pore formation enhanced shedding, suggesting that calcium influx and patch formation enhance repair. In contrast, monomeric toxins were endocytosed. These data indicate that cells use two interrelated mechanisms of membrane repair: lipid-dependent MV shedding, which we term 'intrinsic repair', and patch formation by intracellular organelles. Endocytosis may act after membrane repair is complete by removing inactivated and monomeric toxins from the cell surface.
Cell Death and Differentiation (2017) **24,** 798–808; doi:10.1038/cdd.2017.11; published online 10 February 2017

Pore-forming toxins (PFTs) are utilized by the immune system and pathogens.[1,2] The pathogens *Streptococcus pyogenes*, *Streptococcus intermedius*, and *Clostridium perfringens* produce Streptolysin O (SLO), Intermedilysin (ILY) and Perfringolysin O (PFO), respectively. These toxins are classified as cholesterol-dependent cytolysins (CDCs) because of their need of cholesterol for pore formation.[1] CDCs are secreted as monomers that bind to cholesterol (SLO, PFO) or human CD59 (ILY), then oligomerize into ring-shaped ~30 nm wide prepores and undergo a conformational change that perforates the membrane.[1,3–5] Several mutations arrest pore formation at intermediate stages. SLO G398V/G399V (monomer-locked) locks SLO predominantly as monomers.[6,7] SLO N402E (array-locked) oligomerizes into nontoxic linear arrays.[8,9] SLO Y255A (prepore locked) locks SLO into nontoxic prepores incapable of membrane insertion.[7,10] Finally, SLO N402C has reduced hemolytic activity because it forms a mixture of enlarged, lytic pores, and linear arrays.[8,9] These mutant toxins are valuable tools for understanding cytotoxicity and cellular resistance.

Once inserted, pores undermine cell viability. Cells attempt to reseal tears and remove protein-lined pores through membrane repair.[11,12] The most widely accepted model of membrane repair is 'patch repair'. During patch repair, Ca^{2+} influx depolymerizes cortical actin,[13] recruits annexins to stabilize damaged membranes,[14–17] and promotes fusion of endocytic structures with the damaged membrane.[11] Although well described for mechanical damage and laser wounding,[12,18] it is unclear whether patch repair mediates PFT repair. For PFT repair, two alternative models of repair exist: endocytosis and ectocytosis. In the endocytic model, repair proceeds by rapidly clearing PFTs from the surface by Ca^{2+}-dependent caveolar internalization, and targeting PFTs to lysosomes for degradation.[19,20] However, internalization of active pores, instead of monomers, oligomers or other structures, has yet to be visualized.[19–22] The primary evidence supporting this view is the finding that membrane repair is aborted by methyl-β-cyclodextrin, which disrupts caveolae.[19] However, methyl-β-cyclodextrin alters the lipid homeostasis of the plasmalemma in other profound ways, and is not specific to caveolar internalization.[19]

An alternative model of membrane repair is the reverse process of 'ectocytosis'. In ectocytosis, which occurs with SLO, pneumolysin and MAC, pores are sequestered into membrane blebs and then shed from the cell surface on microvesicles (MVs).[16,23–28] PFT pores are sequestered through an unknown Ca^{2+}-independent mechanism on blebs and tubules,[24,27] which are shed from the membrane in a Ca^{2+}-dependent mechanism.[24] Although Ca^{2+} influx recruits intracellular repair proteins like Annexins[16] and ESCRT-III,[29] it is unclear whether these proteins lead to bleb formation and shedding. Furthermore, any role of membrane lipids in this

[1]Department of Biological Sciences, Texas Tech University, Lubbock, TX, USA; [2]Department of Cell Biology and Physiology, Washington University of Saint Louis, St. Louis, MO, USA and [3]Institute for Integrated Cell-Material Sciences, Kyoto University, Kyoto, Japan

*Corresponding author: PA Keyel, Department of Biological Sciences, Texas Tech University, Biology Room 108, Box 43131, Lubbock, TX 79409-3131, USA. Tel: 806 834 6248; Fax: 806 742 2963; E-mail: peter.keyel@ttu.edu

[4]Current address: Frank Reidy Center for Bioelectrics, Old Dominion University, Norfolk, VA 23529, USA.

[5]Current address: Department of Cell Biology and Biochemistry, Texas Tech University Health Science Center, Lubbock, TX 79430, USA.

Received 29.8.16; revised 13.12.16; accepted 17.1.17; Edited by M Freeman; published online 10.2.2017

process remains to be determined. Thus, the molecular mechanism of this shedding process (and its relationship to patch formation) remains to be determined.

Here we analyzed the mechanism of ectocytosis. We tested the hypothesis that microvesicular shedding is a general mechanism of CDC clearance across multiple cell types using SLO, PFO, and ILY. We found that every cell type examined shed toxin-containing MVs following sublytic CDC challenge. Mechanistically, oligomerization was necessary and sufficient for MV formation, suggesting that eukaryotic cells possess a repair mechanism distinct from patch repair. As this repair mechanism appears to rely on lipid properties intrinsic to the cell membrane, we propose calling this novel ability of membrane lipids to promote shedding following toxin oligomerization 'intrinsic repair'. As pore formation further enhanced shedding beyond that induced by oligomerization, we propose that intrinsic resistance cooperates with patch repair to promote cell survival. In contrast, we found that endocytosis cleared inactive toxin monomers independently membrane repair. Overall, we propose a cohesive model integrating all three models of membrane repair: intrinsic repair sheds toxin pores potentially in concert with patch repair, and once membrane repair is complete, endocytosis restores membrane homeostasis.

Results

Toxin and cell type can dictate CDC resistance. Before testing the hypothesis that active CDCs are cleared by microvesicular shedding, we first needed to determine the sublytic dose for each CDC and if it was equivalent between cell types and CDCs. We compared SLO with ILY, which requires human CD59 for cytotoxicity,[3] and PFO. In order to compare cytotoxicity between toxins, we used a consistent hemolytic dose. This controls for the extremely variable hemolytic activity displayed between PFT preparations, even at the same toxin mass[9,21] (Supplementary Table S1). When normalized by hemolytic activity, we found that all three wild-type toxins, SLO, PFO, and ILY, had equivalent cytotoxicity in HeLa and HEK cells (LD_{50} 500 HU/ml, sublytic dose 125 HU/ml) (Figures 1a and b). To control for impurities in toxin purification, we used an equivalent mass of non-hemolytic monomer-locked SLO.[7] Monomer-locked SLO showed no cytotoxicity (Figures 1a and b). 3T3 cells, one model cell line for membrane repair,[30–32] displayed similar sensitivity to SLO and PFO, but were resistant to ILY, as expected for murine cells (Figure 1c). This indicates a consistent response between cells to neutralize toxin pores.

We next compared these cells with primary murine bone marrow-derived macrophages (BMDMs) and two immune cell lines, THP-1 and NK92MI. In contrast to non-immune cell lines, the immune cell lines showed variability between toxins independently of CD59. THP-1 cells were twofold more sensitive than HeLa cells to ILY (Figure 1d). ILY was not cytotoxic to NK92MI because these cells lack CD59[33] (Figure 1e). NK92MI cells were fourfold more resistant to PFO than HeLa cells (Figure 1e). However, SLO showed similar toxicity in each of these cell lines to HeLa cells (Figure 1). In contrast, BMDM were ~10-fold more resistant to both PFO and SLO (Figure 1f). These results indicate cells can show toxin-specific sensitivity independently of CD59.

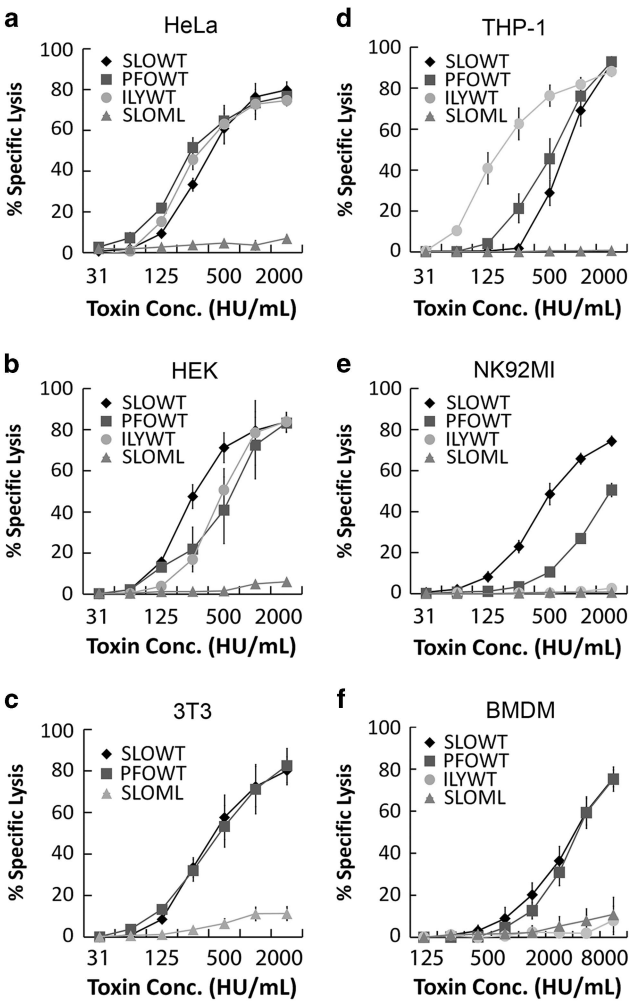

Figure 1 Toxin and cell type dictate CDC resistance. (**a**-**f**) The indicated human and murine cells were challenged with CDCs at the indicated concentrations in 2 mM $CaCl_2$ supplemented RPMI (RC) with 20 μg/ml propidium iodide (PI) for 5 min at 37 °C. PI uptake was analyzed by flow cytometry and specific lysis was determined. The graphs display the average ± S.E.M. of at least three independent experiments

CDC resistance is not determined by CDC binding. Cell-specific sensitivity may be due to differential CDC binding. To test this hypothesis, we used SLO, which showed similar toxicity across all cell lines except BMDM, to control for CDC differences (Figure 1). We conjugated Cy5 to SLO C530A (SLO-Cy5) or monomer-locked SLO C530A (monomer-locked SLO-Cy5), challenged cells and measured binding by flow cytometry. Toxicity to SLO-Cy5 was similar to unconjugated, wild-type SLO, whereas monomer-locked SLO-Cy5 was not cytotoxic (Figure 2a). We found that both SLO-Cy5 and monomer-locked SLO-Cy5 similarly bound all cell types, including highly resistant BMDM, in a dose-dependent manner (Figure 2). Neither toxin saturated binding sites in living cells (Figures 2b and c). These results indicate that saturation of free cholesterol and impairment

of toxin binding are not major factors in cellular resistance to CDCs.

We next asked whether variable resistance within a particular cell population is due to toxin binding. We measured SLO binding in unpermeabilized, transiently permeabilized, and fully lysed cells across a range of SLO-Cy5 concentrations. Both dead and permeabilized cells showed similar toxin binding, typically about 0.5–1 log more toxin than unpermeabilized cells (Figures 2b and c). Interestingly, toxin binding steadily increased in a dose-dependent manner in all subsets until surviving cells at high SLO concentrations bound more toxin than cells killed by lower SLO concentrations (Figure 2b). To control for population changes between each group, we tested whether monomer-locked SLO-Cy5 showed similar binding. This CDC bound similarly to wild-type toxin in all cell types (Figure 2). Thus, toxin binding is unrelated to cellular CDC resistance.

MV shedding acts as general clearance mechanism for CDCs. Although toxin binding was not related to SLO resistance, MV shedding has been related to SLO resistance in HeLa, HEK, and CHO cells.[24,34] We tested if shedding was a general mechanism of CDC resistance. We challenged six cell types with sublytic doses of SLO, ILY, or PFO, or as a negative control, the mass equivalent of monomer-locked SLO, and isolated MV. We found that PFO and SLO localized to MV, whereas ILY was not robustly detected by the anti-SLO antibody (Figure 3). In contrast, monomer-locked SLO did not localize to MV, indicating that toxin monomers do not trigger shedding (Figure 3). Along with active CDCs, we found that the GPI-anchored protein alkaline phosphatase was shed in MV (Figure 3). This finding is consistent with previous results.[24,25] Also consistent with previous results,[16,34] the membrane repair protein Annexin A1 was only present in MV following challenge with cytotoxic CDCs (Figure 3). In contrast, monomer-locked SLO did not promote the shedding of plasma membrane proteins (Figure 3). Overall, we conclude that PFO and ILY are shed similarly to SLO on MV from the plasma membrane.

We next tested if MV represent cellular debris from lysed cells. To test this possibility, we measured the distribution of two nuclear proteins, Lamin A/C and high mobility group box 1 protein (HMGB1). If MV represent cellular debris, Lamin A/C would localize to the supernatant if disassembled, or with MV if it remained associated with the nuclear envelope. In contrast, HMGB1 does not associate with membranes and is released into the supernatant following cell lysis.[35] When we probed for these proteins, Lamin A/C remained in the cell pellet, whereas HMGB1 was present in MV following active CDC challenge, but not in the supernatant (Figure 3). These controls indicate that the MV fraction is not cellular debris. MV typically contain β-actin,[36] and MV are often highly permeabilized,[24] which accounts for the presence of β-actin in all three fractions following treatment with cytotoxic CDCs (Figure 3). We also tested if MV were produced by apoptosis. SLO can induce apoptosis at high toxin concentrations.[37] We found that SLO does not induce apoptosis under our assay conditions, regardless of toxin dose (Supplementary Figure S1). In contrast, UV irradiation induced apoptosis as expected[38] (Supplementary Figure S1). Thus, apoptosis and cell lysis do not account for the observed MV shedding.

Smaller MV induced by SLO and PFO in more resistant cells. To determine whether MV shedding is a conserved repair mechanism between cell types, we compared the cellular responses with sublytic toxin challenges (Figure 3). We observed CDC, alkaline phosphatase, Annexin A1 and HMGB1 in the MV pellet regardless of cell type used (Figure 3). However, cells challenged with monomer-locked SLO or ILY-challenged cells lacking human CD59 did not shed any of these proteins in the MV pellet. These data indicate that MV formation is a general membrane repair response used to eliminate active toxins.

Finally, we used electron microscopy to confirm that the MV fraction comprised membrane-bound structures containing toxin and to measure size of shed vesicles. We observed many membrane-bound structures, which occasionally were positively stained because of charge interactions between stain and lipids.[39] Toxin pores were challenging to detect on MV by negative stain (Figure 4, arrowheads). The majority of MV were 200–400 nm in diameter, with a range of 50–1000 nm, consistent with previous observations.[24] Although most cells had a consistent range of MV sizes, vesicles originating from SLO-treated primary BMDM were typically smaller, ~100–200 nm in diameter (Figure 4). The production of smaller vesicles may be characteristic of cells with robust CDC resistance.

MV formation does not require cytotoxicity. As MV shedding was only triggered by active toxins, it is possible that active pores are shed, whereas inactive toxin is endocytosed. The methods used to assess toxin endocytosis[19–21,40] could not discriminate between active pores and inactive toxin. We tested whether toxin inactivation alters the cellular response to SLO. As wild-type SLO and other CDCs may contain a mixture of active and inactive toxins based on purification and other factors,[26,27] we partially inactivated SLO-Cy5 by freeze–thaw or fully inactivated it by heat treatment. Freeze–thaw reduced cytotoxicity in HeLa cells by twofold, whereas heat treatment eliminated cytotoxicity (Figure 5a). We found that SLO binding did not significantly change between treatments, indicating that toxin binding was not compromised (Figure 5a). Next, we tested how cytotoxic capacity altered membrane shedding by challenging cells with equivalent mass quantities of heat-inactivated SLO. Surprisingly, MV formation was not impaired

Figure 2 CDC resistance is not determined by extent of CDC binding. The indicated cells were resuspended in RC with 20 μg/ml PI, challenged with Cy5 conjugated SLO C530A (SLO WT) or Cy5 conjugated SLO C530A G398V/G399V (SLO ML) at the indicated concentrations for 5 min at 37 °C, analyzed by flow cytometry, and specific lysis (**a**) or toxin binding (**b** and **c**) determined. The graphs display the average ± S.E.M. of at least three independent experiments. *$P < 0.05$. Comparisons between SLO WT and SLO ML, and SLO between cell lines were not significant

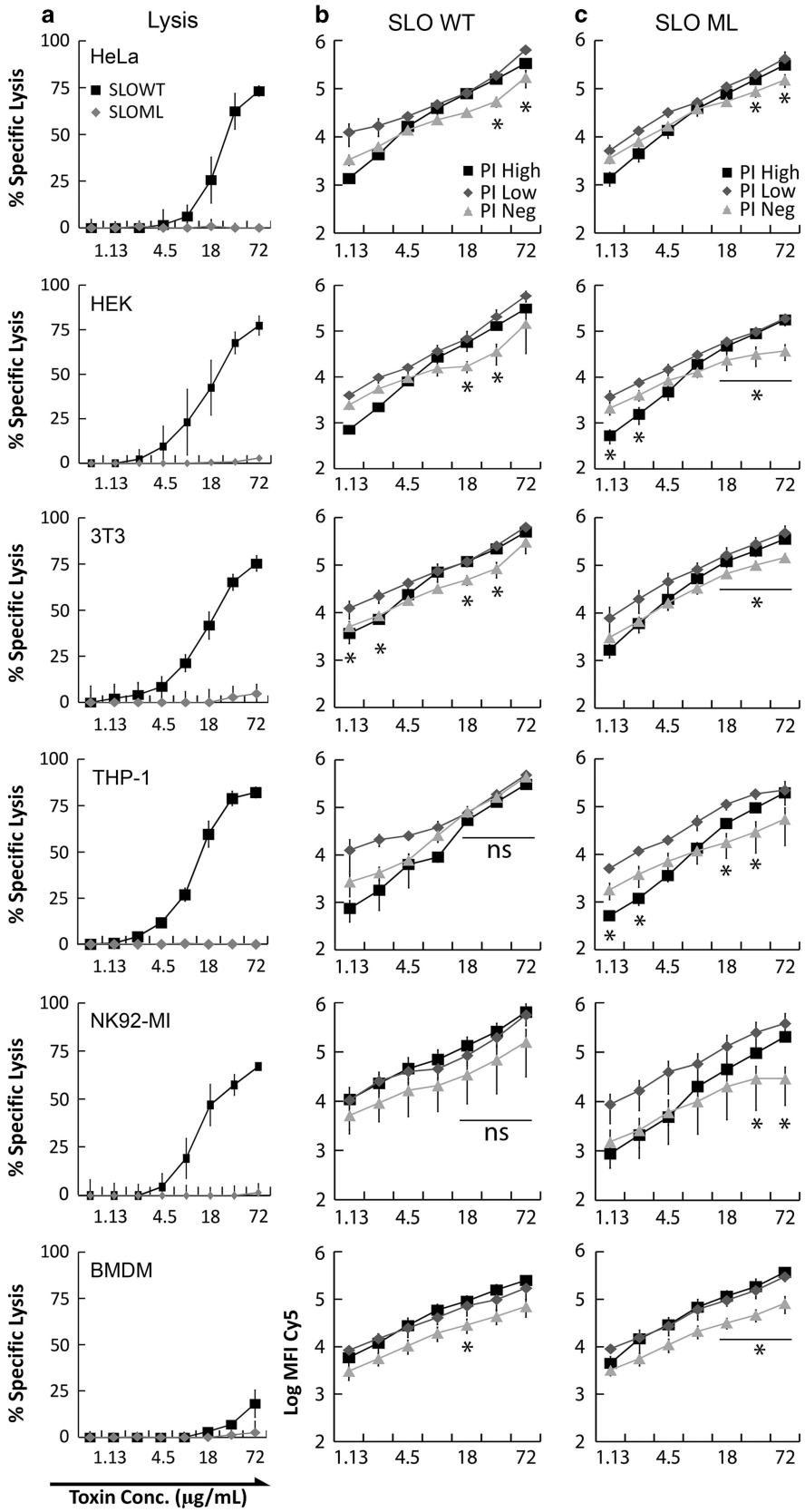
a
Lysis
b
SLO WT
c
SLO ML
HeLa
SLOWT
SLOML
HEK
3T3
THP-1
NK92-MI
BMDM
% Specific Lysis
PI High
PI Low
PI Neg
ns
Log MFI Cy5
Toxin Conc. (μg/mL)
1.13
4.5
18
72

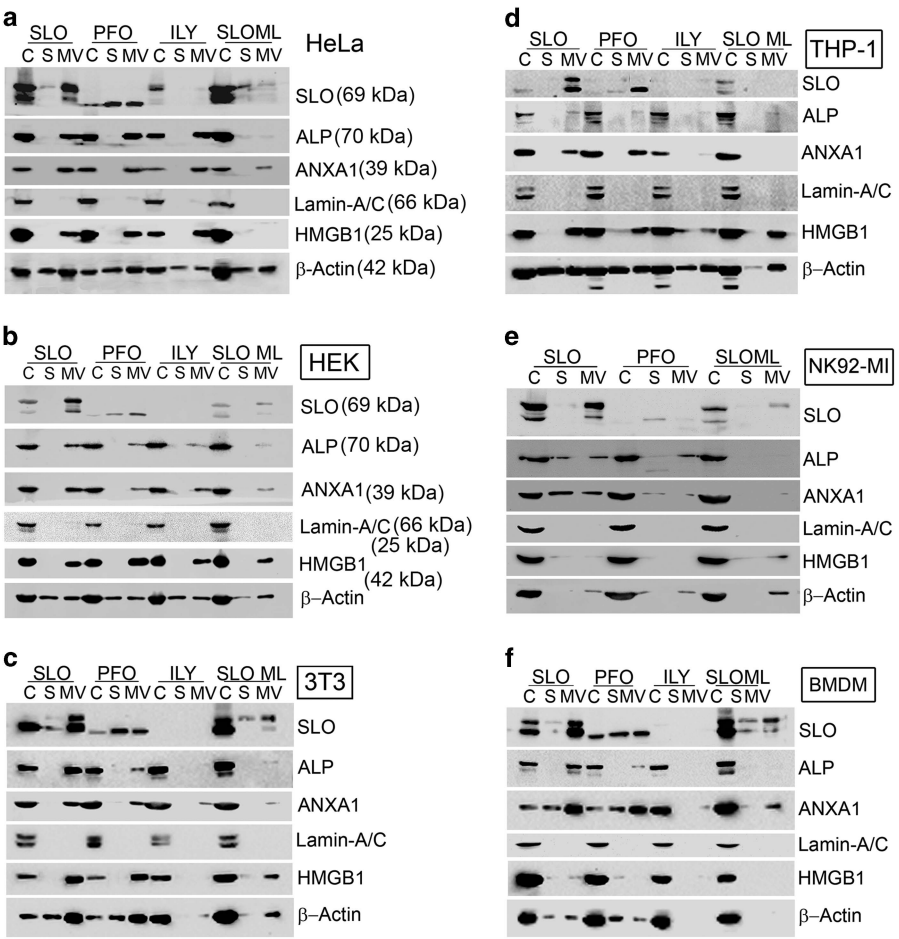

Figure 3 MV shedding acts as a general clearance mechanism for CDCs. The indicated cells were challenged with sublytic concentrations of SLO, PFO, or ILY or equivalent mass of SLO ML in RC for 15 min at 37 °C. Cells were pelleted at 2000 × *g* for 5 min to yield cell pellet (C). Cell supernatants were spun at 100 000 × *g* for 40 min at 4 °C and high-speed supernatant (S) and MV pellet (MV) collected. All fractions were solubilized at 95 °C in SDS-sample buffer, resolved by SDS-PAGE and transferred to nitrocellulose. Portions of the blot were probed with 6D11 anti-SLO, EPR4477 anti-alkaline phosphatase, CPTC-ANXA1–3 anti-Annexin A1, MANLAC-4A7 anti-Lamin A/C, EPR3507 anti-HMGB1 and AC-15 anti-β-actin antibodies. ILY did not reliably cross-react with 6D11, so it is not consistently visualized on blots. The blots show one representative experiment from at least three independent experiments

by heat inactivation, as HeLa cells robustly shed SLO, alkaline phosphatase and Annexin A1 in MV regardless of SLO activity (Figure 5b). However, HMGB1 secretion in MV required pore formation (Figure 5b). These results suggest that membrane shedding does not require membrane perforation or intracellular repair mechanisms such as patch repair.

Toxin oligomerization is necessary and sufficient for membrane shedding. As heat-inactivated SLO was shed, but monomer-locked SLO was not, we tested whether oligomerization was sufficient to promote MV shedding using toxins arrested at different stages of oligomerization.[7,9] As these toxins are non-hemolytic, we tested whether they showed cytotoxicity at equivalent masses to wild-type SLO. We found that array-locked and prepore-locked SLO neither killed HeLa cells nor promoted transient permeabilization (Figures 6a and b). We tested whether these toxins promoted MV formation by treating cells with a sublytic dose of wild-type SLO or mass equivalent of mutant SLO. Although monomer-locked SLO did not promote MV shedding, both array-locked and prepore-locked SLO induced MV formation (Figure 6c). These data show that toxin oligomerization is necessary and sufficient to promote membrane shedding. These data further suggest that patch repair is not required for MV shedding. This suggests that MV shedding represents a new mechanism of CDC elimination, which we term intrinsic repair.

If intrinsic repair is a protective mechanism triggered by toxin oligomerization, then we predict addition of non-hemolytic toxin oligomers will enhance cellular survival following CDC challenge. To test this prediction, we used SLO N402C, which forms a mixture of enlarged, competent pores and oligomeric linear arrays. It has ~10-fold lower specific activity than wild-type SLO against erythrocytes.[9] If linear arrays promote membrane repair, we expect SLO N402C will have reduced cytotoxicity at equivalent hemolytic doses. Indeed, we found that SLO N402C was poorly cytotoxic at all doses, in contrast to wild-type SLO (Figure 6d).

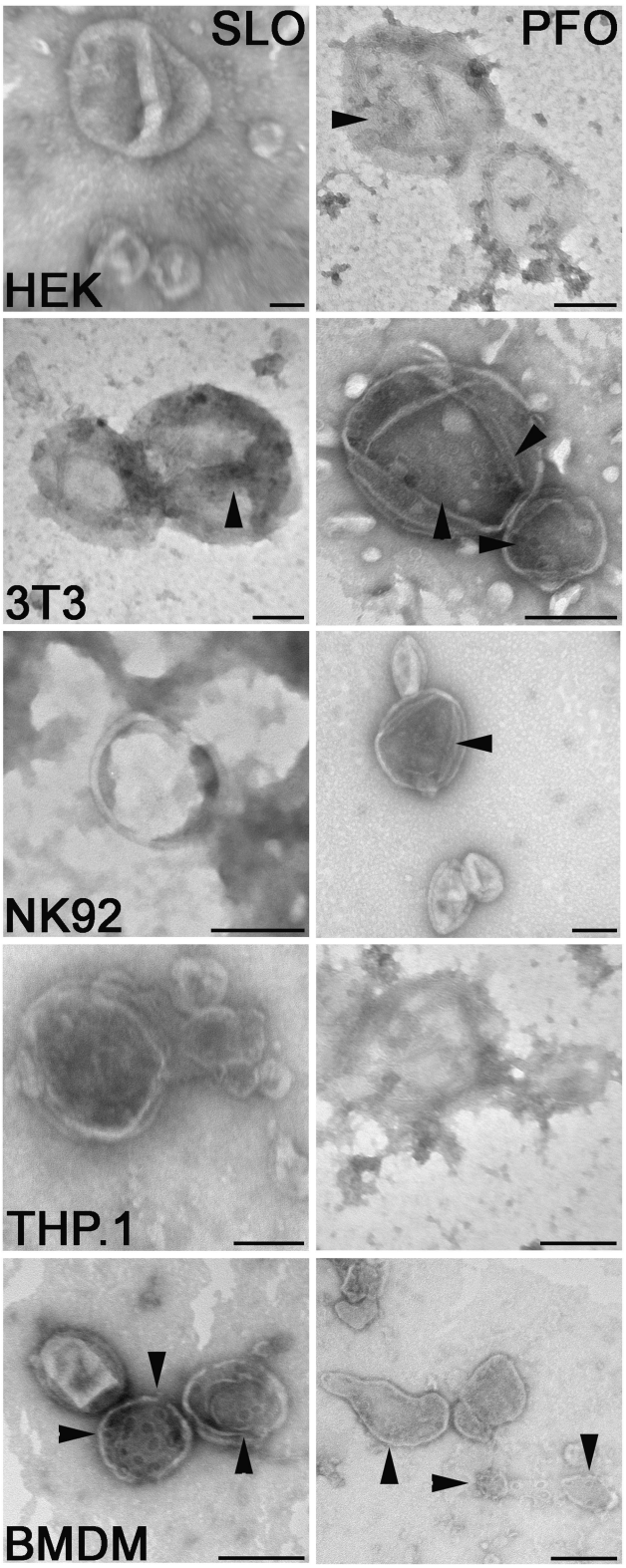

Figure 4 Membrane blebs exhibit structural similarity. The indicated cells were challenged with a sublytic concentration of SLO or PFO in RC for 15 min to induce membrane blebbing. MVs were recovered by ultracentrifugation as described in Figure 3, adsorbed onto formavar-coated grids, negatively stained using 1% uranyl acetate, and visualized using transmission electron microscopy. Representative micrographs from three independent experiments are shown. Arrowheads mark CDC pores. Scale bar = 200 nm

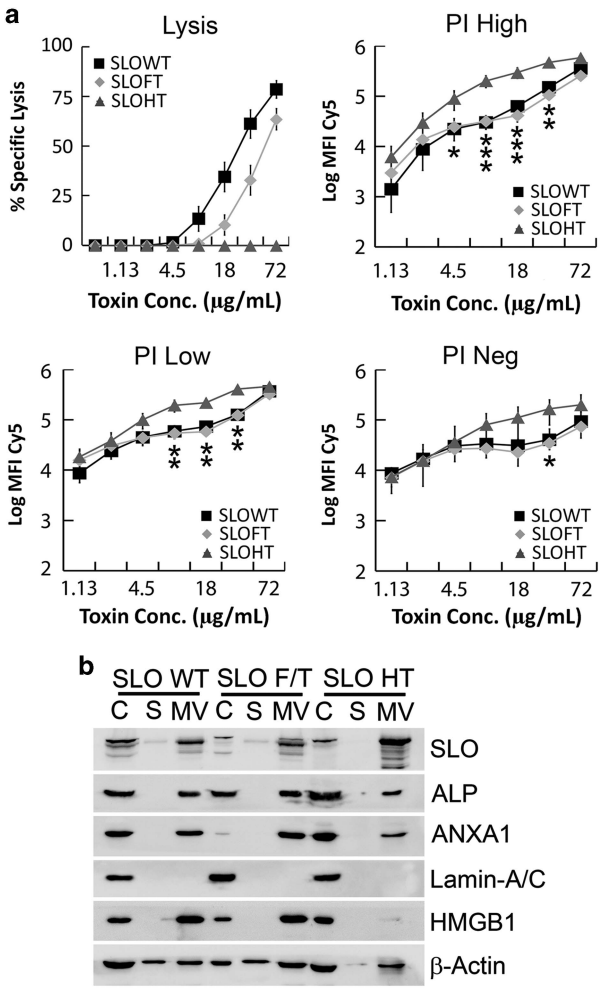

Figure 5 MV formation does not require cytotoxicity. Cy5 conjugated SLO C530A was partially inactivated by freeze–thaw (SLO FT), fully inactivated by heat treatment at 37 °C for 15 min (SLO HT) or left unperturbed (SLO WT). (**a**) Cells were resuspended in RC with 20 μg/ml PI and challenged with equivalent masses of all three toxin subsets. (**b**) MV were isolated as described in Figure 3 from cells challenged with 250 HU/ml SLO WT or equivalent masses of other toxins. Graphs display the average $\pm$ S.E.M., whereas blots show one representative experiment, of at least three independent experiments. *$P<0.05$, **$P<0.01$ and ***$P<0.001$

SLO N402C transiently permeabilized cells, confirming that pore formation occurred (Figure 6e). As one hallmark of membrane repair is calcium dependence,[11,12,31,41] we tested whether calcium removal altered repair following SLO N402C challenge. We challenged HeLa cells with wild-type SLO or SLO N402C in the presence of EGTA and measured PI uptake. We observed that the absence of calcium made cells about twofold more sensitive to wild-type SLO (Figure 6d). Given the extremely low cytotoxicity of SLO N402C, we observed no increase in cytotoxicity (Figure 6d). However, we observed an increase in cell permeabilization (Figure 6e). This

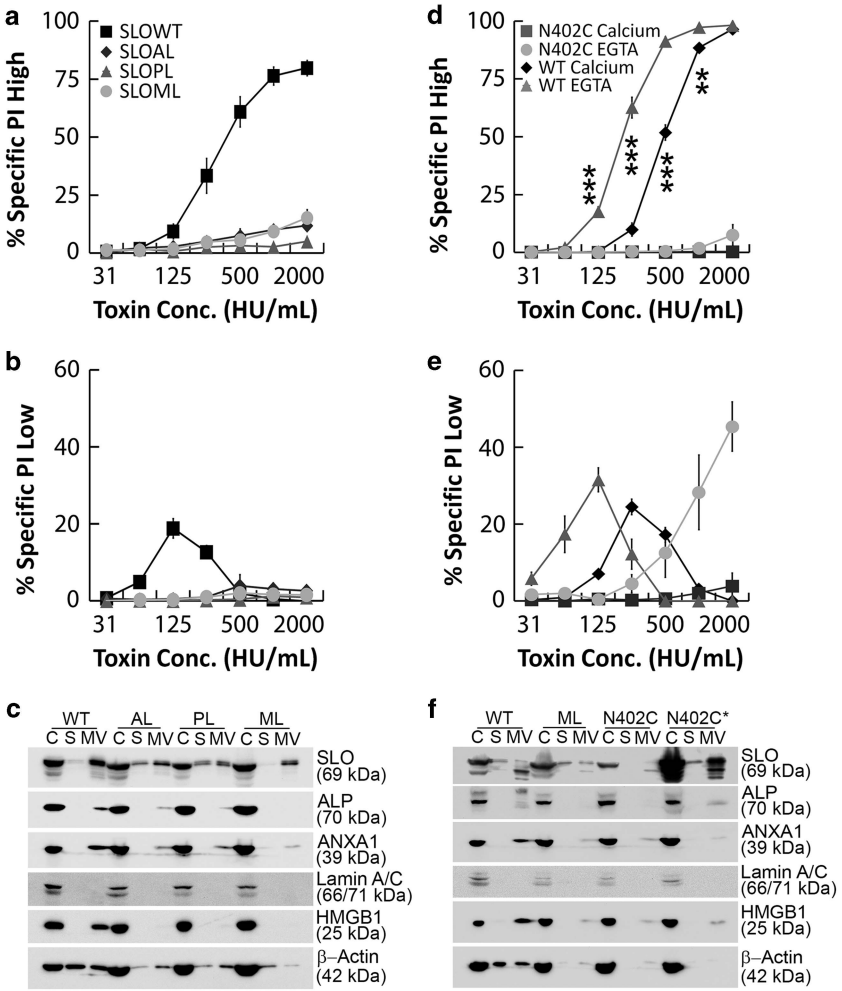

Figure 6 Toxin oligomerization is necessary and sufficient for membrane shedding. (**a** and **b**) HeLa cells were challenged with SLO WT, SLO ML, SLO N402E 'array-locked' (SLO AL), or SLO Y255A 'prepore locked' (SLO PL) at the indicated concentrations in RC with 20 μg/ml PI for 5 min at 37 °C. PI uptake was analyzed by flow cytometry and specific lysis (**a**) or permeabilization (**b**) was determined. (**c**) MV from HeLa cells challenged with a sublytic dose of SLO WT or mass equivalent of other toxins were isolated and probed as described in Figure 3. (**d** and **e**) HeLa cells were challenged with SLO WT or SLO N402C (N402C) in either RC (calcium) or 2 mM EGTA in RPMI (EGTA) with PI for 5 min at 37 °C. PI uptake was analyzed by flow cytometry and specific lysis (**d**) or permeabilization (**e**) was determined. (**f**) MV from HeLa cells challenged with a sublytic dose of SLO, mass equivalent of SLO ML or SLO N402C, or equivalent hemolytic activity of SLO N402C (N402C*) were isolated and probed as described in Figure 3. Graphs display the average ± S.E.M. of at least three independent experiments. Blots show one representative experiment from at least three independent experiments. $^{**}P<0.01$ and $^{***}P<0.001$

indicates that SLO N402C promotes robust calcium-dependent repair. Finally, we measured MV production induced by SLO N402C both at equivalent mass and equivalent hemolytic activity to wild-type SLO. Although an equivalent mass of SLO N402C induced less robust shedding than wild-type SLO, treatment with an equivalent hemolytic dose of SLO N402C induced a similar degree of shedding (Figure 6f). We interpret these results to indicate that addition of inactive linear arrays decreases CDC cytotoxicity, which enhances repair. Furthermore, as the combination of active pores and inactive oligomers promoted increased shedding compared with inactive oligomers alone, we believe that membrane perforation triggers additional repair events beyond intrinsic repair, potentially patch repair. Thus, intrinsic repair and patch repair may cooperate for optimal membrane repair.

Compensatory endocytosis only removes inactive SLO from the cell surface. As shedding removes both active pores and inactive oligomers, we determined the fate of monomer-locked SLO, which is not shed. We tested whether monomer-locked SLO is removed by endocytosis. We incubated HeLa cells with dextran concurrently with wild-type SLO or monomer-locked SLO and examined them by immunofluorescence. Wild-type SLO localized to a few punctate structures (Figure 7a), as previously described.[19,24] In contrast, an equivalent mass of monomer-locked SLO localized more broadly across the cells (Figure 7b), consistent with our observation that wild-type SLO is shed from cells, but monomer-locked SLO remains cell associated (Figure 3). As the endocytosis model suggests an increase in endocytosis following SLO challenge, we next compared the number of dextran-positive structures in each treatment

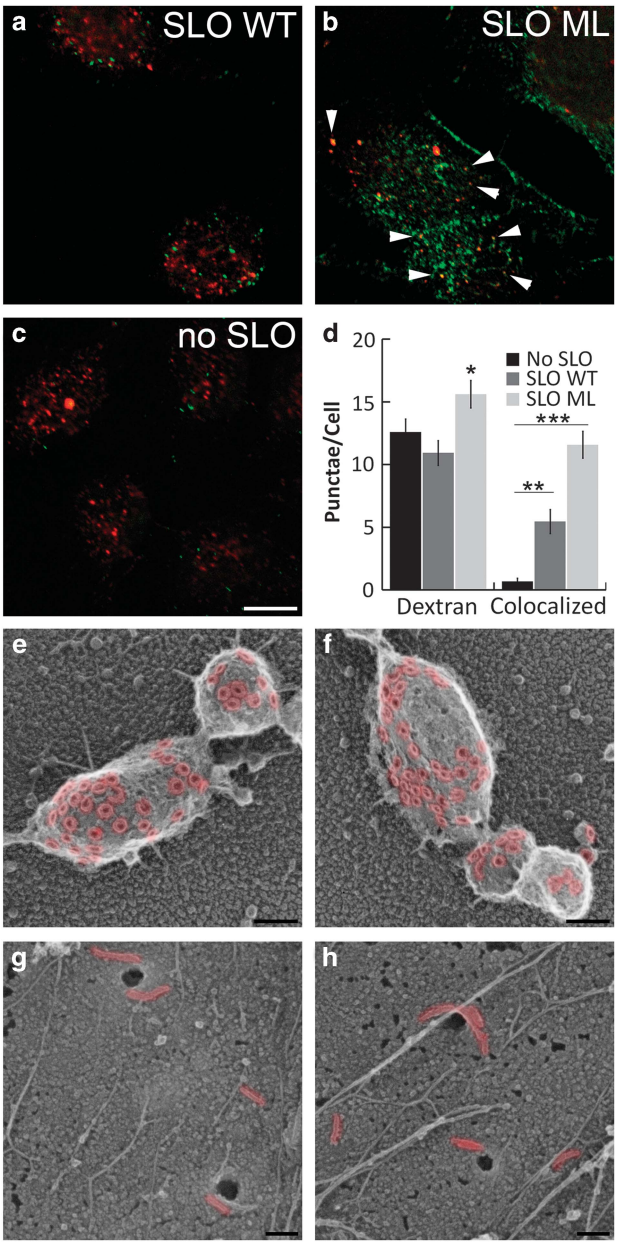

Figure 7 Compensatory endocytosis removes inactive SLO from the cell surface. (**a**–**d**) HeLa cells were seeded onto coverslips, serum starved for 1 h in RPMI and challenged with sublytic dose of SLO WT (**a**), the equivalent mass of SLO ML (**b**), or no toxin (**c**) in the presence of 2.5 mg/ml dextran Texas Red (red) in RC for 15 min at 37 °C. Coverslips were fixed, permeabilized, and stained with 6D11 anti-SLO antibody followed by anti-mouse 488 antibody, mounted and analyzed by confocal microscopy. (**d**) The number of dextran punctae and dextran/SLO double-positive punctae was quantified by direct counts. (**e**–**h**) HeLa cells were seeded onto coverslips, challenged with a sublytic dose of SLO (**e** and **f**) or mass equivalent of SLO ML (**g** and **h**) for 5 min at 37 °C, washed, fixed in 2% glutaraldehyde and analyzed by rapid-freeze, 'deep-etch' EM. SLO pores and oligomers are pseudo-colored red to aid visualization. Immunofluorescent images show one representative image of five independent experiments. The graph displays the average ± S.E.M. of five independent experiments. EM micrographs show representative fields from two independent experiments. $^{*}P<0.05$, $^{**}P<0.01$ and $^{***}P<0.001$. Scale bar = 10 μm for (**a**–**c**) and 100 nm for (**e**–**h**)

group (Figures 7a–c). On average, we found 15.6 ± 1.1 dextran-positive punctae/cell in cells challenged with monomer-locked SLO, whereas we found 12.6 ± 1.0 and 10.9 ± 0.99 punctae/cell in unchallenged and wild-type SLO challenged cells, respectively (Figure 7d). This suggests that monomer-locked SLO, but not wild-type SLO, promotes endocytosis. We next determined the extent of colocalization between SLO and dextran. Wild-type SLO colocalized with dextran much less frequently than monomer-locked SLO, with 5.46 ± 0.96 colocalized punctae/cell compared with 11.6 ± 1.1 punctae/cell with monomer-locked SLO (Figure 7d). This suggests that inactive, monomeric SLO is cleared by endocytosis, whereas active pores are cleared via MV shedding.

As immunofluorescence does not reveal pore architecture or ultrastructure, we cannot discriminate between SLO/dextran punctae that represent blebs on the surface or SLO/dextran punctae that represent endosomes, nor can we discriminate monomers from linear arrays or complete pores. Although monomer-locked SLO is predominantly monomeric,[6,7] short oligomers are also formed by this toxin.[6,7] In order to directly visualize SLO pore architecture and cellular ultrastructure, we used rapid-freeze 'deep-etch' electron microscopy to visualize SLO on HeLa cells (Figures 7e–h). We observed high concentrations of complete pores sequestered on membrane blebs on HeLa cells challenged with wild-type SLO (Figures 7e and f). We attribute cell-associated wild-type SLO detected by flow cytometry (Figure 2), western blot (Figure 3), and immunofluorescence (Figure 7a) to SLO on these blebs. In contrast, we observed short oligomers of monomer-locked SLO widely distributed on the plasma membrane, and no toxin sequestered on blebs (Figures 7g and h). Monomer-locked SLO instead localized to endocytic pits on the cell surface (Figures 7g and h). Therefore, previously described endocytosis of SLO[19] could represent the internalization of SLO monomers and short oligomers. This suggests a new model for membrane repair (Figure 8). Overall, we propose that resistance to CDC pores and oligomers relies on intrinsic repair – sequestration and membrane shedding – coupled to recruitment of repair proteins and patch formation, whereas monomeric toxins and unshed blebs are cleared after repair by compensatory endocytosis (Figure 8).

Discussion

We examined the mechanism of membrane repair using multiple bacterial toxins and cell lines. We found toxin and cell type both controlled lethality independently of toxin binding. At sublytic toxin doses, we found that all cell types executed membrane repair through microvesicular shedding, with smaller vesicles associated with improved repair. We found that endocytosis acts after repair to remove inactive toxin from the membrane. This suggests a model in which membrane repair acts in two coordinated steps: intrinsic repair and patch formation. Intrinsic repair of the cell membrane was triggered by toxin oligomerization, whereas pore formation enhanced repair, suggesting patch repair may also contribute to CDC clearance. Overall, these results provide a new paradigm for membrane repair of CDC-induced damage.

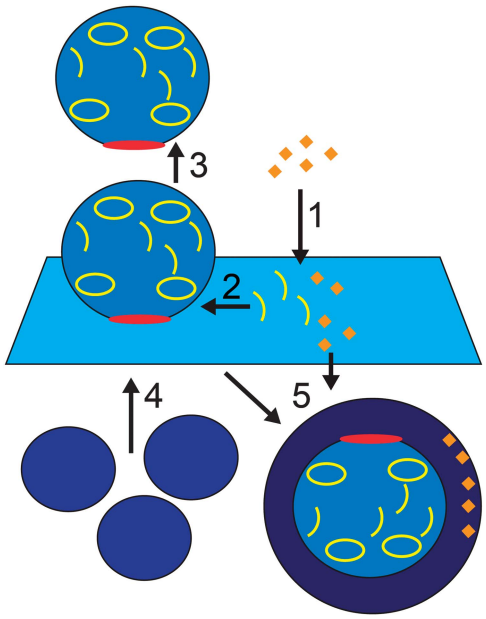

Figure 8 Membrane repair acts by intrinsic repair and patch formation. (1) Toxin monomers bind to cholesterol or human CD59 on the cell membrane and oligomerize. (2) Oligomerization drives sequestration of toxin on blebs via intrinsic repair. Blebs can be sealed by repair proteins (red) like Annexins, or catalyzed by ESCRT machinery. (3) MVs are shed from the membrane in a Ca^{2+}-dependent manner. (4) Intracellular vesicles undergo Ca^{2+} -dependent patch formation with the plasma membrane to complete resealing. (5) Once repair is complete, endocytosis restores membrane homeostasis by clearing unshed toxin-laden blebs and monomeric toxins

We found that SLO, PFO, and ILY are all shed on MV from a range of cell types spanning primary murine macrophages to immortalized human cell lines. These findings add to the extensive body of evidence from multiple groups showing that cells resist PFTs via MV shedding.[16,23–27,42,43] Despite this evidence, it has been argued that MAC,[22,44] perforin,[21] and SLO[19,20] are resisted by endocytosis. These arguments have relied on methods which cannot discriminate between monomeric and oligomeric toxin. Our ultrastructural evidence suggests an explanation that reconciles these seemingly opposed observations. We find that inactive toxin is endocytosed, whereas complete pores are sequestered on blebs for shedding. Our findings indicate that sequestration and shedding is the primary resistance mechanism, whereas compensatory endocytosis removes inactive toxin and toxin-laden blebs once repair is complete.

Our finding that toxin oligomerization is necessary and sufficient for MV shedding have far-reaching implications. It implies that specific toxin activity is critical to interpreting membrane repair experiments. Our experiments with heat-inactivated and mutant toxins suggest that repair responses can be altered by the specific activity of the toxin preparation. Recently, it was shown that pneumolysin is robustly shed.[27] Notably, this toxin had low-specific activity (87 kHU/mg *versus* 450–1280 kHU/mg for SLO here) and was 90% prepores.[27] Both of these factors may account for the robust shedding and survival. Similarly, the non-hemolytic PFT Ostreolysin A promotes blebbing at high concentrations.[45] The switch to blebbing could depend on the extent of oligomerization. Overall, our findings support a stronger role for lipid membrane dynamics in membrane repair than previously appreciated.

Finally, our findings suggest a new model of membrane repair. We propose that membrane repair acts in two steps: intrinsic repair and patch formation. Intrinsic repair is the ability of the lipid bilayer to resist PFTs based on the biochemical and biophysical properties of the membrane lipids, like sterol accessibility[46] or sequestration of toxin oligomers onto blebs. Neither ATP nor proteins[24] are necessary for intrinsic repair, although lipid modifying and binding enzymes, especially sphingomyelinases, likely enhance and regulate intrinsic repair. In conjunction with intrinsic repair, calcium influx through pores promotes shedding and marshals an intracellular response.[24] Repair proteins, including Annexins and ESCRT machinery, are recruited to sites of damage.[12,14,16,29] These proteins act to seal the damage and facilitate patch repair: the hetero/homotypic fusion of intracellular vesicles with the plasma membrane.[17] Both forms of repair act in concert to quickly restore membrane homeostasis. Compensatory endocytosis has a functionally distinct role in our model by clearing inactive toxin, blebs that failed to shed, and intracellular components after repair. This model reconciles seemingly contradictory observations and provides a framework for understanding the relationships between repair proteins and membrane lipids involved in membrane repair. Future research will examine whether non-CDCs trigger intrinsic repair, how CDC-induced lipid reorganization leads to blebbing, how shedding kinetics are regulated, and the coordination between intrinsic repair and patch formation.

Materials and Methods

Reagents. All reagents were from Thermofisher Scientific (Waltham, MA, USA) unless otherwise noted. The pBAD-gIII plasmid encoding His-tagged SLO[7] was a kind gift from Michael Caparon (Washington University in St. Louis, MO, USA). Cysteine-less His-tagged PFO in pET22[47] and Cysteine-less His-tagged ILY in pTrcHisA,[48] respectively, were generous gifts from Rodney Tweten (University of Oklahoma Health Sciences Center, Oklahoma City, OK, USA). Monomer-locked (G398V/G399V) and prepore-locked (Y255A) SLO were generated by Quikchange PCR. Primer sequences are available upon request. Cysteine-less SLO (C530A), array-locked (N402E), and N402C SLO were previously described.[9] Anti-Annexin A1 (CPTC-ANXA1-3-s) was deposited to the DSHB by Clinical Proteomics Technologies for Cancer (DSHB Hybridoma Product CPTC-ANXA1-3) and anti-Lamin A/C (MANLAC-4A7-s) was deposited to the DSHB by GE Morris (DSHB Hybridoma Product MANLAC1(4A7)). Both were obtained from the Developmental Studies Hybridoma Bank, created by the NICHD of the NIH and maintained at the University of Iowa, Department of Biology, Iowa City, IA, USA. Anti-alkaline phosphatase EPR4477 rabbit monoclonal antibody (rAb) (catalog: GTX62596) and anti-β-actin AC-15 mouse monoclonal antibody (mAb) (catalog: GTX26276) were obtained from GeneTex (Irvine, CA, USA). Anti-SLO antibody 6D11 mAb (catalog: NBP1–05126) was obtained from Novus Biologicals (Littleton, CO, USA). Anti-HMGB1 EPR3507 rAb (catalog: ab79823) was obtained from Abcam (Cambridge, MA, USA). Anti-mouse (711-035-151) and anti-rabbit (711-035-152) HRP-conjugated antibodies were obtained from Jackson Immunoresearch (West Grove, PA, USA).

Mice. All mice were housed and maintained at Texas Tech University according to IACUC standards, adhering to the Guide for the Care and Use of Laboratory Animals (8th edn, NRC 2011) for animal husbandry. C57BL/6 mice were purchased from the Jackson Laboratory (Bar Harbor, ME, USA) (stock # 000664). Mice of both genders aged 6–15 weeks were used to prepare BMDM. Sample size was determined as the minimum number of mice needed to provide sufficient bone marrow for experiments. Consequently, no randomization or blinding was needed. Mice were killed by asphyxiation through controlled flow of pure CO_2 followed by cervical dislocation.

Cell culture. All cell lines were maintained at 37 °C, 5% CO_2. HeLa (ATCC (Manassas, VA, USA) CCL-2), HEK-293 (ATCC CRL-1573), and THP-1 cells (ATCC TIB-202) were cultured in DMEM (Corning, Corning, NY, USA) supplemented with 10% fetal calf serum (FCS) (Atlas Biologicals, Fort Collins, CO, USA) and 1x L-glutamine (D10). 3T3 cells (ATCC, CRL-1658) and L929 cells (ATCC, CCL1) were cultured in D10 supplemented with 1 mM sodium pyruvate (Corning) and 1x non-essential amino acids (GE Healthcare, Pittsburgh, PA, USA). NK92MI cells (ATCC, CRL-2408) were cultured in Alpha MEM (GE Healthcare) supplemented with 10% FCS, 1x L-glutamine, 0.2 mM myo-inositol and 0.02 mM folic acid. Macrophages were isolated from C57BL/6 mouse bone marrow and cultured as previously described.[49] BMDM were differentiated for 7–21 days in DMEM supplemented with 30% L929 cell supernatants, 20% FCS (VWR Seradigm, Radnor, PA, USA), 1 mM sodium pyruvate and 1x L-glutamine.

Recombinant toxins. Toxins were purified as previously described.[26] Toxins were induced with 0.2% arabinose (SLO), or 0.2 mM IPTG (PFO and ILY). For conjugation of toxins to Cy5, purified toxin was gel filtered into 100 mM sodium bicarbonate (pH 8.5) using a Zeba gel filtration column according to the manufacturer's instructions. Enough monoreactive Cy5 dye (GE Healthcare) to label 0.25 mg protein was reconstituted 100 mM sodium bicarbonate, added to the recombinant SLO and incubated at room temperature for 1 h. Conjugated SLO was gel filtered into PBS to remove unconjugated dye and 5 mM DTT was added before snap freezing on dry ice. The C530A mutation retains wild-type binding, pore structure, and hemolytic activity, but removes oxygen sensitivity of the toxin.[9,50] Removal of oxygen sensitivity is critical for Cy5 conjugation, as Cy5 conjugation of oxygen-sensitive toxin greatly reduces hemolytic activities in an unpredictable manner (data not shown). Protein concentration was determined by Bradford Assay and hemolytic activity was determined as previously described.[26] Instead of sheep red blood cells, human red blood cells (ZenBio, Research Triangle Park, NC, USA) were used. One hemolytic unit is defined as the amount of toxin required to lyse 50% of a 2% human red blood cell solution after 30 min at 37 °C in 2 mM $CaCl_2$, 10 mM HEPES and 0.3% BSA in PBS. The specific activity and protein concentrations for each active toxin is listed in Supplementary Table S1. We used HU/ml to normalize toxin activities in each experiment and to achieve consistent cytotoxicity across toxin preparations. Pore-deficient toxins SLO G398V/G399V (SLO monomer-locked), SLO Y255A (SLO prepore locked), and SLO N402E (SLO array locked) had a specific activity of <10 HU/mg. For freeze–thaw and heat treatment experiments, one aliquot of SLO was thawed, a portion removed to assess wild-type cytotoxicity and the remainder frozen at -20 °C for 5 min. Once thawed, a portion was removed to assess cytotoxicity of freeze-thawed toxin and the remainder incubated at 37 °C for 15 min before assessing cytotoxicity of heat-inactivated toxin.

Cytotoxicity assay. Cytotoxicity was assessed as previously described.[24] Cells were resuspended in 200 μl at 2×10^6 cells/ml in RPMI supplemented with 2 mM $CaCl_2$ (RC) and 20 μg/ml propidium iodide (Sigma, St. Louis, MO, USA). We maintained a consistent number of cells and assay volume instead of normalizing to cellular protein because intracellular protein does not directly correlate with cellular surface area. As cells were in suspension and rounded, surface area correlates with forward scatter (FSC) by flow cytometry (Supplementary Table S2). We found that toxin sensitivity did not correlate with FSC, suggesting that total surface area did not have a role in our system. In some experiments, the 2 mM $CaCl_2$ was replaced with 2 mM EGTA. Toxins were diluted in RC according to hemolytic activity (wild-type toxins) or equivalent mass (inactive mutant toxins) and further diluted in twofold intervals. Cells were examined for PI fluorescence using an Accuri C6 (BD Biosciences, San Jose, CA, USA). Debris was gated out and cells exhibiting high PI fluorescence (2–3 log shift) (PI high), low PI fluorescence (~1 log shift) (PI low), or background PI fluorescence (PI neg) were quantified, normalized against untreated cells, and graphed according to toxin concentration. Both PI neg and PI low populations remain metabolically active, indicating that only the PI high population are dead cells.[24] Specific lysis was determined as follows: % Specific Lysis = (% PI $High_{Experimental}$—% PI $High_{Control}$)/(100—%PI $High_{Control}$). Permeabilized cells were determined similarly, using PI Low instead of PI High populations. The sublytic dose was defined as the highest toxin concentration that gave $<20\%$ specific lysis.

Annexin V assay. HeLa cells (5×10^5) were challenged with SLO at various concentrations for 30 min at 37 °C or UV irradiated for 15 s followed by 4 h culture at 37 °C. Following treatment, cells were stained with 0.9 μg/ml Annexin V-FITC and 20 μg/ml PI in Annexin V Binding Buffer (1.4 mM NaCl, 25 mM $CaCl_2$, 100 mM HEPES, pH 7.4) for 15 min on ice and analyzed by FACS using an Accuri C6.

Isolation of MVs. MV were isolated as previously described.[24] Briefly, 5×10^6–1×10^7 cells were harvested, resuspended in RC at 2.5×10^6–5×10^6 cells/ml, challenged with a sublytic concentration of toxin (hemolytic toxins) or equivalent mass (inactive toxins) and incubated for 15 min at 37 °C. Cells were pelleted at $2000\times g$ for 5 min, solubilized at 95 °C in SDS-sample buffer for 5 min and sonicated. Supernatants were spun at $100\,000\times g$ in a Beckman Coulter TL-100 ultracentrifuge using a Beckman TLS 55 rotor for 40 min at 4 °C. Both high-speed supernatant and MV pellet were solubilized at 95 °C in 4x SDS-sample buffer. We label these structures as 'microvesicles' to distinguish them from exosomes and other extracellular vesicles. Exosomes are 40–120 nm cup-shaped structures derived from the lumen of multivesicular bodies, whereas MVs are variably sized plasma membrane derived vesicles.[51] We have previously demonstrated [24,52,53] that vesicles triggered by SLO best fit the definition of MVs. These MV are also not toxic to cells and do not fuse with the plasma membrane of cells that internalize these MV.[52,53]

SDS-PAGE and immunoblotting. Samples were resolved on 10% polyacrylamide gels at 90 V/165 min and transferred in ice bath to nitrocellulose in transfer buffer (15.6 mM Tris and 120 mM glycine) at 90 mA for 85 min. Blocking was performed using 5% skim milk in 10 mM Tris-HCl, 150 mM NaCl and 0.1% Tween 20 at pH 7.5. Blots were incubated with 6D11 anti-SLO mAb (1:1000), CPTC-ANXA1–3 anti-Annexin A1 (1:250) mAb, MANLAC-4A7 anti-Lamin A/C (1:250) mAb, AC-15 anti-β-actin (1:5000) mAb, EPR3507 anti-HMGB1 (1: 4000) rAb, or EPR4477 anti-alkaline phosphatase rAb (1:1000) followed by HRP-conjugated anti-mouse or anti-rabbit IgG antibodies (1:10,000) and developed with ECL (0.01% H_2O_2 (Walmart, Fayetteville, AR, USA), 0.2 mM p-Coumaric acid (Sigma), 1.25 mM Luminol (Sigma), 0.1 M Tris pH 8.4).[54]

Electron microscopy. MV were isolated by ultracentrifugation as described above, resuspended in PBS, and adsorbed onto formavar-coated grids for 5 min. Grids were negatively stained using 1% uranyl acetate for 30 s and imaged on a Hitachi (Tokyo, Japan) H-8100 transmission electron microscopy. Rapid-freeze, 'deep-etch' microscopy was performed as previously described.[9,24]

Immunofluorescence. Immunofluorescence was performed as previously described.[24] HeLa cells were plated on coverslips, serum starved in RPMI for 1 h at 37 °C, challenged with SLO diluted in RPMI containing 2.5 mg/ml 10 000 MW lysine-fixable dextran Texas Red and 2 mM $CaCl_2$ for 15 min at 37 °C. Cells were washed in PBS, fixed in 2% paraformaldehyde, washed, permeabilized in 10% goat serum with 0.02% saponin, probed with 6D11 anti-SLO (1:250) mAb for 1 h, washed, probed with goat Alexa-Fluor-488-conjugated anti-mouse-IgG (1:500) for 1 h, washed, DAPI stained, washed and mounted on slides in gelvatol. Cells were imaged on a Fluoview 300 confocal microscope (Olympus, Waltham, MA, USA) using a 63x oil objective (1.40 NA) and CoolSnap HQ2 camera (Photometrics, Tucson, AZ, USA). Images were quantitated using Photoshop (Adobe, San Jose, CA, USA).

Statistics. Prism 5.0 (Graphpad, La Jolla, CA, USA) or SPSS (IBM, Armonk, NY, USA) were used for statistical analysis. Data are represented as mean $\pm$ S.E.M. as indicated. Statistical significance was determined by two-way ANOVA with Bonferroni post-testing; $P<0.05$ was considered statistically significant. Graphs were generated in Excel (Microsoft, Redmond, WA, USA) and Photoshop.

Conflict of Interest

The authors declare no conflict of interest.

Acknowledgements. We thank Kai Zhang for use of his flow cytometer and the College of Arts and Sciences Microscopy (Lubbock, TX, USA) for use of their facilities. We thank Rodney Tweten and Michael Caparon for plasmids. This work was supported by Texas Tech University start-up funds and American Heart Association grant (16SDG302000016) to PAK. The funders had no role in experimental design, analysis, and interpretation of data; preparation of the manuscript; nor in the decision to submit the article for publication.

1. Tweten RK, Hotze EM, Wade KR. The unique molecular choreography of giant pore formation by the cholesterol-dependent cytolysins of Gram-positive bacteria. *Annu Rev Microbiol* 2015; **69**: 323–340.
2. Gilbert RJ, Mikelj M, Dalla Serra M, Froelich CJ, Anderluh G. Effects of MACPF/CDC proteins on lipid membranes. *Cell Mol Life Sci* 2013; **70**: 2083–2098.

3. Giddings KS, Zhao J, Sims PJ, Tweten RK. Human CD59 is a receptor for the cholesterol-dependent cytolysin intermedilysin. *Nat Struct Mol Biol* 2004; **11**: 1173–1178.
4. Rossjohn J, Polekhina G, Feil SC, Morton CJ, Tweten RK, Parker MW. Structures of perfringolysin O suggest a pathway for activation of cholesterol-dependent cytolysins. *J Mol Biol* 2007; **367**: 1227–1236.
5. Tilley SJ, Orlova EV, Gilbert RJ, Andrew PW, Saibil HR. Structural basis of pore formation by the bacterial toxin pneumolysin. *Cell* 2005; **121**: 247–256.
6. Ramachandran R, Tweten RK, Johnson AE. Membrane-dependent conformational changes initiate cholesterol-dependent cytolysin oligomerization and intersubunit [beta]-strand alignment. *Nat Struct Mol Biol* 2004; **11**: 697–705.
7. Magassa NG, Chandrasekaran S, Caparon MG. Streptococcus pyogenes cytolysin-mediated translocation does not require pore formation by streptolysin O. *EMBO Rep* 2010; **11**: 400–405.
8. Abdel Ghani EM, Weis S, Walev I, Kehoe M, Bhakdi S, Palmer M. Streptolysin O: inhibition of the conformational change during membrane binding of the monomer prevents oligomerization and pore formation. *Biochemistry* 1999; **38**: 15204–15211.
9. Keyel PA, Roth R, Yokoyama WM, Heuser JE, Salter RD. Reduction of Streptolysin O (SLO) pore-forming activity enhances inflammasome activation. *Toxins* 2013; **5**: 1105–1118.
10. Hotze EM, Wilson-Kubalek EM, Rossjohn J, Parker MW, Johnson AE, Tweten RK. Arresting pore formation of a cholesterol-dependent cytolysin by disulfide trapping synchronizes the insertion of the transmembrane beta-sheet from a prepore intermediate. *J Biol Chem* 2001; **276**: 8261–8268.
11. McNeil PL, Kirchhausen T. An emergency response team for membrane repair. *Nat Rev Mol Cell Biol* 2005; **6**: 499–505.
12. Cooper ST, McNeil PL. Membrane repair: mechanisms and pathophysiology. *Physiol Rev* 2015; **95**: 1205–1240.
13. Miyake K, McNeil PL, Suzuki K, Tsunoda R, Sugai N. An actin barrier to resealing. *J Cell Sci* 2001; **114**: 3487–3494.
14. Demonbreun AR, Quattrocelli M, Barefield DY, Allen MV, Swanson KE, McNally EM. An actin-dependent annexin complex mediates plasma membrane repair in muscle. *J Cell Biol* 2016; **213**: 705–718.
15. Bouter A, Gounou C, Berat R, Tan S, Gallois B, Granier T *et al.* Annexin-A5 assembled into two-dimensional arrays promotes cell membrane repair. *Nat Commun* 2011; **2**: 270.
16. Babiychuk EB, Monastyrskaya K, Potez S, Draeger A. Blebbing confers resistance against cell lysis. *Cell Death Differ* 2011; **18**: 80–89.
17. McNeil AK, Rescher U, Gerke V, McNeil PL. Requirement for Annexin A1 in plasma membrane repair. *J Biol Chem* 2006; **281**: 35202–35207.
18. McNeil PL, Miyake K, Vogel SS. The endomembrane requirement for cell surface repair. *Proc Natl Acad Sci USA* 2003; **100**: 4592–4597.
19. Corrotte M, Almeida PE, Tam C, Castro-Gomes T, Fernandes MC, Millis BA *et al.* Caveolae internalization repairs wounded cells and muscle fibers. *eLife* 2013; **2**: e00926.
20. Idone V, Tam C, Goss JW, Toomre D, Pypaert M, Andrews NW. Repair of injured plasma membrane by rapid Ca2+-dependent endocytosis. *J Cell Biol* 2008; **180**: 905–914.
21. Keefe D, Shi LF, Feske S, Massol R, Navarro F, Kirchhausen T *et al.* Perforin triggers a plasma membrane-repair response that facilitates CTL induction of apoptosis. *Immunity* 2005; **23**: 249–262.
22. Moskovich O, Herzog L-O, Ehrlich M, Fishelson Z. Caveolin-1 and Dynamin-2 are essential for removal of the complement C5b-9 complex via endocytosis. *J Biol Chem* 2012; **287**: 19904–19915.
23. Scolding NJ, Morgan BP, Houston WAJ, Linington C, Campbell AK, Compston DAS. Vesicular removal by oligodendrocytes of membrane attack complexes formed by activated complement. *Nature* 1989; **339**: 620–622.
24. Keyel PA, Loultcheva L, Roth R, Salter RD, Watkins SC, Yokoyama WM *et al.* Streptolysin O clearance through sequestration into blebs that bud passively from the plasma membrane. *J Cell Sci* 2011; **124**(Pt 14): 2414–2423.
25. Xie M, Low MG. Streptolysin-O induces release of glycosylphosphatidylinositol-anchored alkaline phosphatase from ROS cells by vesiculation independently of phospholipase action. *Biochem J* 1995; **305**(Pt 2): 529–537.
26. Keyel PA, Heid ME, Watkins SC, Salter RD. Visualization of bacterial toxin induced responses using live cell fluorescence microscopy. *J Vis Exp* 2012; **68**: 4227.
27. Wolfmeier H, Radecke J, Schoenauer R, Koeffel R, Babiychuk VS, Drucker P *et al.* Active release of pneumolysin prepores and pores by mammalian cells undergoing a Streptococcus pneumoniae attack. *Biochim Biophys Acta* 2016; **1860**: 2498–2509.
28. Moskovich O, Fishelson Z. Live cell imaging of outward and inward vesiculation induced by the complement c5b-9 complex. *J Biol Chem* 2007; **282**: 29977–29986.
29. Jimenez AJ, Maiuri P, Lafaurie-Janvore J, Divoux S, Piel M, Perez F. ESCRT machinery is required for plasma membrane repair. *Science* 2014; **343**: 986-+.
30. Miyake K, McNeil PL. Vesicle accumulation and exocytosis at sites of plasma membrane disruption. *J Cell Biol* 1995; **131**: 1737–1745.
31. Bi GQ, Alderton JM, Steinhardt RA. Calcium-regulated exocytosis is required for cell membrane resealing. *J Cell Biol* 1995; **131**: 1747–1758.
32. Shen SS, Tucker WC, Chapman ER, Steinhardt RA. Molecular regulation of membrane resealing in 3T3 fibroblasts. *J Biol Chem* 2005; **280**: 1652–1660.
33. Marcenaro E, Augugliaro R, Falco M, Castriconi R, Parolini S, Sivori S *et al.* CD59 is physically and functionally associated with natural cytotoxicity receptors and activates human NK cell-mediated cytotoxicity. *Eur J Immunol* 2003; **33**: 3367–3376.
34. Babiychuk EB, Monastyrskaya K, Potez S, Draeger A. Intracellular Ca2+ operates a switch between repair and lysis of streptolysin O-perforated cells. *Cell Death Differ* 2009; **16**: 1126–1134.
35. Yang H, Rivera Z, Jube S, Nasu M, Bertino P, Goparaju C *et al.* Programmed necrosis induced by asbestos in human mesothelial cells causes high-mobility group box 1 protein release and resultant inflammation. *Proc Natl Acad Sci USA* 2010; **107**: 12611–12616.
36. Muralidharan-Chari V, Clancy JW, Sedgwick A, D'Souza-Schorey C. Microvesicles: mediators of extracellular communication during cancer progression. *J Cell Sci* 2010; **123**: 1603–1611.
37. Timmer AM, Timmer JC, Pence MA, Hsu LC, Ghochani M, Frey TG *et al.* Streptolysin O promotes group A Streptococcus immune evasion by accelerated macrophage apoptosis. *J Biol Chem* 2009; **284**: 862–871.
38. Dunkern TR, Fritz G, Kaina B. Ultraviolet light-induced DNA damage triggers apoptosis in nucleotide excision repair-deficient cells via Bcl-2 decline and caspase-3/-8 activation. *Oncogene* 2001; **20**: 6026–6038.
39. Wyffels JT. Principles and techniques of electron microscopy: biological applications, fourth edition, by M. A. Hayat. *Microsc Microanal* 2001; **7**: 66.
40. Carney DF, Koski CL, Shin ML. Elimination of terminal complement intermediates from the plasma membrane of nucleated cells: the rate of disappearance differs for cells carrying C5b-7 or C5b-8 or a mixture of C5b-8 with a limited number of C5b-9. *J Immunol* 1985; **134**: 1804–1809.
41. Terasaki M, Miyake K, McNeil PL. Large plasma membrane disruptions are rapidly resealed by Ca2+-dependent vesicle-vesicle fusion events. *J Cell Biol* 1997; **139**: 63–74.
42. Wiedmer T, Sims PJ. Participation of protein kinases in complement C5b-9-induced shedding of platelet plasma membrane vesicles. *Blood* 1991; **78**: 2880–2886.
43. Morgan BP, Dankert JR, Esser AF. Recovery of human neutrophils from complement attack: removal of the membrane attack complex by endocytosis and exocytosis. *J Immunol* 1987; **138**: 246–253.
44. Carney DF, Hammer CH, Shin ML. Elimination of terminal complement complexes in the plasma membrane of nucleated cells: influence of extracellular Ca2+ and association with cellular Ca2+. *J Immunol* 1986; **137**: 263–270.
45. Skočaj M, Resnik N, Grundner M, Ota K, Rojko N, Hodnik V *et al.* Tracking cholesterol/sphingomyelin-rich membrane domains with the Ostreolysin A-mCherry protein. *PLoS ONE* 2014; **9**: e92783.
46. Das A, Brown MS, Anderson DD, Goldstein JL, Radhakrishnan A. Three pools of plasma membrane cholesterol and their relation to cholesterol homeostasis. *eLife* 2014; **3**: e02882.
47. Shepard LA, Heuck AP, Hamman BD, Rossjohn J, Parker MW, Ryan KR *et al.* Identification of a membrane-spanning domain of the thiol-activated pore-forming toxin Clostridium perfringens perfringolysin O: an alpha-helical to beta-sheet transition identified by fluorescence spectroscopy. *Biochemistry* 1998; **37**: 14563–14574.
48. Giddings KS, Johnson AE, Tweten RK. Redefining cholesterol's role in the mechanism of the cholesterol-dependent cytolysins. *Proc Natl Acad Sci USA* 2003; **100**: 11315–11320.
49. Heid ME, Keyel PA, Kamga C, Shiva S, Watkins SC, Salter RD. Mitochondrial reactive oxygen species induces NLRP3-dependent lysosomal damage and inflammasome activation. *J Immunol* 2013; **191**: 5230–5238.
50. Pinkney M, Beachey E, Kehoe M. The thiol-activated toxin streptolysin O does not require a thiol group for cytolytic activity. *Infect Immun* 1989; **57**: 2553–2558.
51. Raposo G, Stoorvogel W. Extracellular vesicles: exosomes, microvesicles, and friends. *J Cell Biol* 2013; **200**: 373–383.
52. Keyel PA, Heid ME, Salter RD. Macrophage responses to bacterial toxins: a balance between activation and suppression. *Immunol Res* 2011; **50**: 118–123.
53. Keyel PA, Tkacheva OA, Larregina AT, Salter RD. Coordinate stimulation of macrophages by microparticles and TLR ligands induces foam cell formation. *J Immunol* 2012; **189**: 4621–4629.
54. Yakunin AF, Hallenbeck PC. A luminol/iodophenol chemiluminescent detection system for western immunoblots. *Anal Biochem* 1998; **258**: 146–149.

Supplementary Information accompanies this paper on Cell Death and Differentiation website (http://www.nature.com/cdd)